Holographically patterned activation using photo-absorber induced neural–thermal stimulation

2013 J. Neural Eng. 10 056004

(http://iopscience.iop.org/1741-2552/10/5/056004)

J. Neural Eng. **10** (2013) 056004 (11pp) doi:10.1088/1741-2560/10/5/056004

Holographically patterned activation using photo-absorber induced neural–thermal stimulation

Nairouz Farah[1,3], **Alaa Zoubi**[1,3], **Suhail Matar**[1,3], **Lior Golan**[1], **Anat Marom**[1], **Christopher R Butson**[2], **Inbar Brosh**[1] and **Shy Shoham**[1,4]

[1] Faculty of Biomedical Engineering, Technion—Israel Institute of Technology, Haifa 32000, Israel
[2] Departments of Neurology and Neurosurgery, Medical College of Wisconsin, Milwaukee, WI, USA

E-mail: sshoham@bm.technion.ac.il

Received 25 February 2013
Accepted for publication 9 July 2013
Published 31 July 2013
Online at stacks.iop.org/JNE/10/056004

Abstract

Objective. Patterned photo-stimulation offers a promising path towards the effective control of distributed neuronal circuits. Here, we demonstrate the feasibility and governing principles of spatiotemporally patterned microscopic photo-absorber induced neural–thermal stimulation (PAINTS) based on light absorption by exogenous extracellular photo-absorbers.
Approach. We projected holographic light patterns from a green continuous-wave (CW) or an IR femtosecond laser onto exogenous photo-absorbing particles dispersed in the vicinity of cultured rat cortical cells. Experimental results are compared to predictions of a temperature-rate model (where membrane currents follow $I \propto \mathrm{d}T/\mathrm{d}t$). *Main results.* The induced microscopic photo-thermal transients have sub-millisecond thermal relaxation times and stimulate adjacent cells. PAINTS activation thresholds for different laser pulse durations (0.02 to 1 ms) follow the Lapicque strength-duration formula, but with different chronaxies and minimal threshold energy levels for the two excitation lasers (an order of magnitude lower for the IR system <50 nJ). Moreover, the empirical thresholds for the CW system are found to be in good agreement with detailed simulations of the temperature-rate model, but are generally lower for the IR system, suggesting an auxiliary excitation mechanism. *Significance*. Holographically patterned PAINTS could potentially provide a means for minimally intrusive control over neuronal dynamics with a high level of spatial and temporal selectivity.

S Online supplementary data available from stacks.iop.org/JNE/10/056004/mmedia

(Some figures may appear in colour only in the online journal)

1. Introduction

Recent years have seen the emergence of applied optical neuro-stimulation, primarily driven by the introduction of two promising neural photo-stimulation technologies: optogenetic stimulation using light-sensitive ion channels and pumps [1] and direct infrared neural stimulation (INS) [2–4]. Despite the tremendous promise of optogenetic photo-stimulation tools, stable transduction is currently only obtainable through viral transfection, and may face the substantial barriers currently faced by other gene-therapy approaches prior to its clinical application. INS presents an alternative, potentially more direct and simple path to light-mediated neuro-stimulation in various neural tissues using near-IR laser pulses tuned to water-absorption peaks around 2 μm. Effective stimulation using this approach was demonstrated, for example, in peripheral nerves [5], cranial nerves (facial [6], auditory [7] and vestibular [8, 9]),

[3] These authors contributed equally to this work.
[4] Author to whom any correspondence should be addressed.

and in the central nervous system (CNS) [10]. Of the probable mechanisms mediating INS excitation (electric-field mediated, photo-mechanical and photo-thermal), the most likely appears to be photo-thermal [11, 12]. The thermal transient resulting from the absorption of IR light pulse by the tissue's water content putatively causes rapid membrane capacitance changes and induced currents that lead to neural excitation [13, 14], although the modulation of mitochondrial Ca^{+2} transport may also be involved [9]. However, when photo-thermal stimulation is considered for applications requiring an interface with deep or three-dimensional structures, e.g., for vision restoration strategies based on patterned stimulation of downstream systems like the optic nerve [15], thalamus [16] and visual cortex [17], the technology requires adaptations that will allow the use of light at wavelengths that can pass through unaffected brain tissue with *minimal* intrinsic absorption and scattering and that can be readily patterned in space and time.

To adapt photo-thermal excitation to the requirements of such systems we developed photo-absorber induced neural–thermal stimulation or PAINTS, a method which replaces water-based absorption (which only occurs at the tissue's outer surface) with microscopic thermal transients induced by effective photo-absorbers (here, black micro-particles with $\sim$6 μm diameter) scattered in the extra-cellular space in close proximity to the target cells. The photo-absorbers absorb light energy and transfer it to heat, which in turn activates the cells in their near vicinity (a related non-optical method for neuro-thermal stimulation uses radio-frequency heating of magnetic nano-particles to remotely activate temperature-sensitive cation channels [18]). Conceptually, PAINTS can be viewed as a hybrid between INS and the use of exogenously introduced photo-sensitization in optogenetics, except that in principle any tissue-compatible extrinsic [19] or intrinsic light absorbers can be used. This alternative photo-thermal strategy can use light with flexible wavelengths: here we use light in the visible range (532 nm) and 800 nm near-IR light (which is very weakly absorbed and scattered in cortical tissue); both wavelengths can be readily combined with high spatiotemporal resolution projection systems, including current spatial light modulators (SLMs) for generating computer-controlled holographic patterns. Computer-generated holography [20–22] is uniquely suited to photo-thermal excitation by allowing parallel stimulation of multiple points at high local light intensities with millisecond-scale temporal precision.

Here, we provide a first proof-of-concept illustration that holographic photo-thermal stimulation can drive patterned neural activity and study the stimulation thresholds in a number of neuronal preparations (extending our earlier unpublished reports of this approach [14, 23, 24]). In addition, as part of the efforts towards understanding the mechanism underlying thermal neural stimulation we test the hypothesis wherein temperature transients induce an inward transmembrane stimulation current which is proportional to their time derivative ($I \propto \mathrm{d}T/\mathrm{d}t$). An opposite, inverse temperature-rate model (where $I \propto -\mathrm{d}T/\mathrm{d}t$) was previously derived by Barnes [25] from Nernst equilibrium relations, in his attempt to explain the thermal effects induced by electromagnetic radiation deposition on neurons; however, this model cannot explain the *depolarizing* current occurring during INS [12, 13]. A temperature-rate model may explain why slow temperature changes fail to excite cells while fast thermal transients induced by short laser pulses succeeded, as well as the fact that activation seems to be independent of baseline temperature [11]. We find that our experimental results display a good agreement with the predictions of the temperature-rate model when using short pulses of a continuous-wave (CW) laser, while markedly lower thresholds are seen when using an ultrafast pulsed IR laser, suggesting the possible involvement of an additional auxiliary excitation mechanism.

2. Methods

2.1. Holographic projection systems

To achieve targeted activation of cells, computer controlled holographic projection systems based on phase-modulating SLMs were used in two different wavelengths and optical setups. A green CW laser pattern was projected through an inverted microscope and an IR femtosecond laser was projected through a custom upright microscope.

Green CW inverted holographic system (HS I). In this system [20] (figure 1(a)), a diode pumped solid state green laser 532 nm (5-532-DPSS-1.0, Altechna) is expanded by a 1:4 beam expander (Keplerian telescope) and projected onto a fast binary ferroelectric SLM with 1280 $\times$ 1024 pixels (SXGA-R3, ForthDD, Scotland; only the 512 $\times$ 512 central pixels are used in order to speed up calculations, at the expense of a larger spot size). The SLM image is then projected onto the objective back aperture by a 2:1 demagnifying telescope comprising a 400 mm plano-convex lens and the microscope tube lens (f = 200 mm). Projection through a plan fluor 20 $\times$ /0.5 objective (Nikon, Japan) yields a FOV of roughly 310 μm with a spot size of approximately 5 μm. To control the light intensity in consecutive pulses, the weighted Gerchberg–Saxton hologram generating algorithm [26] with the appropriate weights was used, except for pulses shorter than the SLM's temporal resolution (0.5 ms), where a static image was projected and calibrated analogue laser modulation was performed instead.

IR *femtosecond upright holographic system (HS II).* The projection system used for infrared activation experiments (figure 1(b)) is based on a custom-built two-photon laser scanning microscope with a Titanium-Sapphire laser source (MaiTai WB, Spectra Physics, average power <1.5 W, 180 fs pulses, 800 nm) which was modulated by a Pockels cell (350-80LA, Conoptics, shortest pulse duration $\sim$10 μs) and relayed to the microscope. The laser beam was expanded by a telescope (65 mm scan lens and 125 mm lens) before being phase-modulated by an SLM positioned at an oblique angle of 15° (XY Phase DMP512, Boulder Nonlinear Systems). The modulated beam was relayed through a 1:1 telescope onto a 60 $\times$, 1.0 NA water-immersion objective lens (NIR Apo, Nikon), which projected the desired pattern onto the biological sample (spot dimensions: $\sim$600 nm lateral FWHM, and $\sim$3.2 μm axial FWHM). Two polarizing half-wave plates (AHWP05-950, Thorlabs) were inserted in the optical path

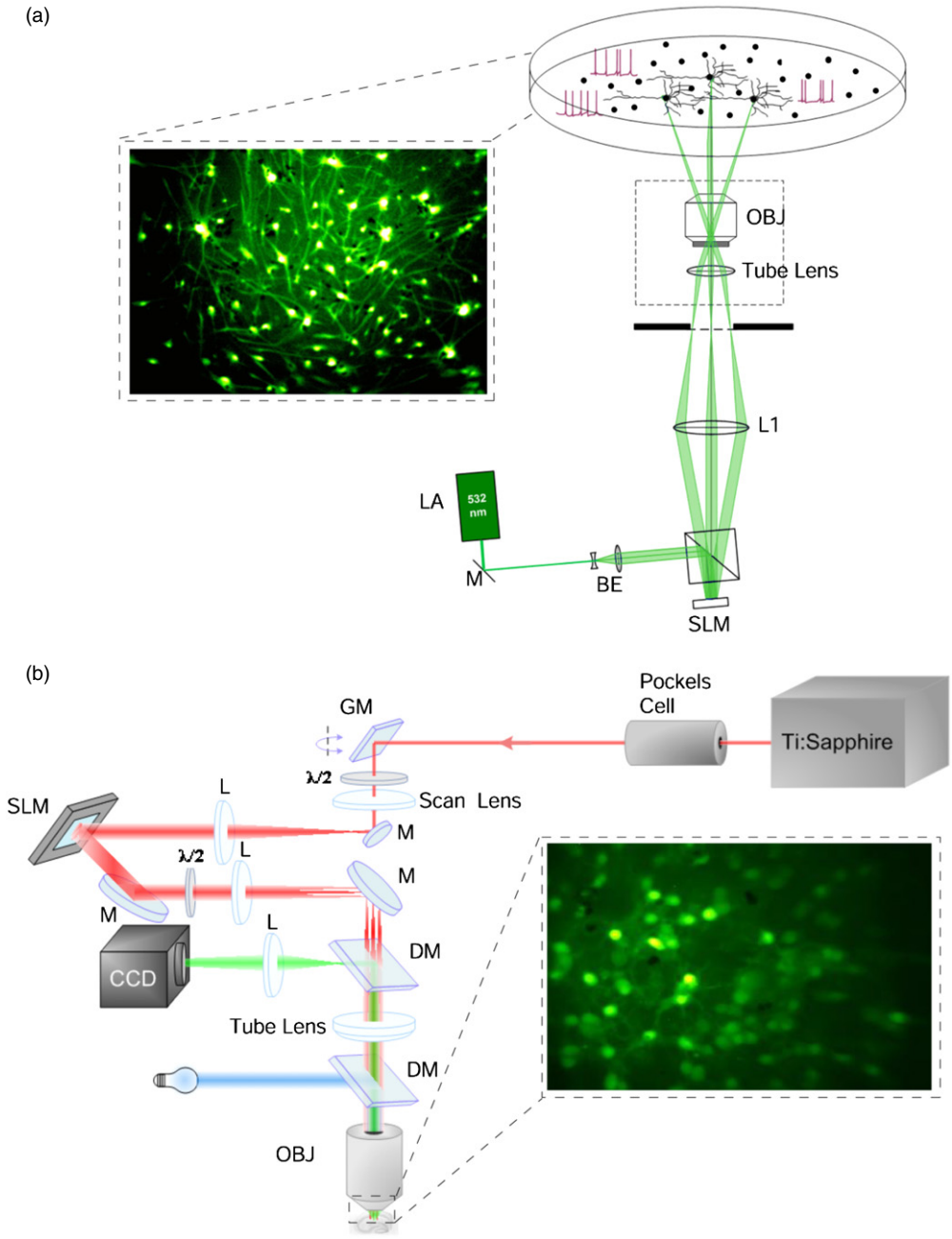

Figure 1. Holographic projection systems. (a) A schematic diagram of HS I: the green laser (LA) beam passes through a mirror (M) and a beam expander (BE), and a polarizing beam splitter before being reflected off a spatial light modulator (SLM). The modulated beam is projected through a demagnifying telescope (L1 and tube lens), and the microscope's objective lens (OBJ) onto the neural preparation. Inset: cell culture preparation with dispersed micro-particles stained with the calcium indicator OGB1. (b) Layout of HS II: the IR laser beam's power is controlled by a Pockels cell, before being relayed onto the SLM, and then imaged onto the objective lens' back aperture. Wide-field fluorescence images are collected using IR-transmitting dichroic mirrors (DM). Inset: slice culture preparation with dispersed micro-particles stained with the calcium indicator Fluo4.

in order to match the SLM polarization direction, and to maximize transmission through the dichroic mirrors. For imaging, we used a fibre illuminator (Intensilight C-HGFI, Nikon) and a CCD camera (GC1380 H, Prosilica).

2.2. Tissue preparations and experimental protocol

Animal experiments and procedures were approved by the Institutional Animal Care Committee at Technion—Israel Institute of Technology and were in accord with the NIH Guide for the Care and Use of Laboratory Animals.

To study photo-thermal activation of cortical neurons, intense light patterns generated using the digital holography systems described above were directed onto particles dispersed in the vicinity of rat cortical cells in two different *in vitro* culture preparations stained with calcium-sensitive fluorescent dyes. Calcium transients induced by photo-thermal stimulation

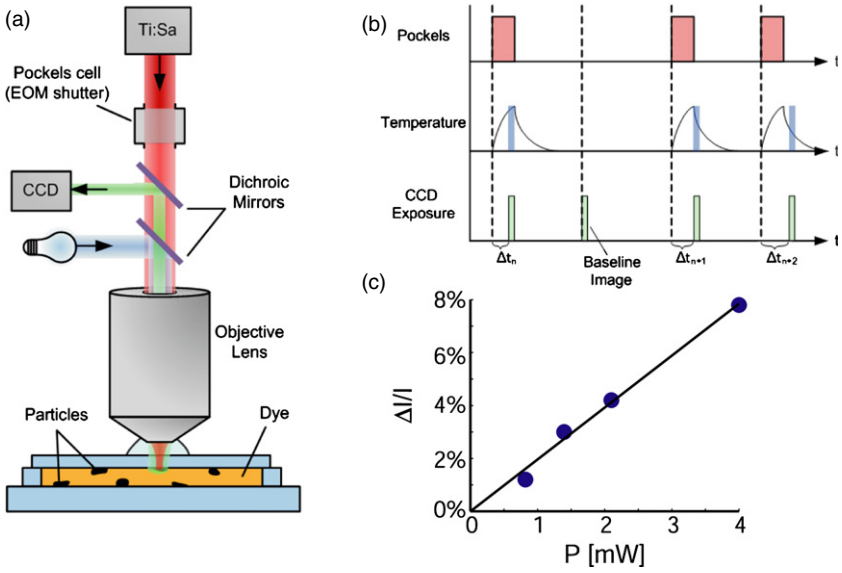

Figure 2. FMI setup. (a) Layout of optical setup used for FMI measurements at HS II: the laser beam is shuttered by an electro-optic modulator (a Pockels Cell) and imaged onto a thin layer of tris(2,2'-bipyridine)ruthenium(II) in which photo-absorbing particles were scattered. A fluorescent lamp provides constant, wide-field illumination, while a CCD camera is used to capture images of the fluorescent signal. (b) General scheme of an FMI measurement: a specific photo-absorber is targeted and is repeatedly exposed to the laser at a fixed rate large enough to avoid heat build-up between successive repetitions. For each repetition, the unchanging temperature profile generated is sampled at a varying delay from the pulse's onset by snapping a short-exposure image of the affected fluorescent signal around a particle using the CCD. Every few cycles, the laser exposure is skipped, providing baseline images which enable bleaching compensation. (c) Linear dependence of peak $\Delta I/I$ as a function of illumination power.

were imaged and stimulation power thresholds for varying pulse durations were measured.

2.2.1. Cell cultures. Cortical tissue was obtained from 0–2 days old Sprague Dawley rats. Cells were plated on polyethyleneimine coated coverslips, onto which micron-scale absorbers (iron oxide based, HP LaserJet) were first dispersed, and experiments were performed 1–3 weeks after plating the primary culture. The cell cultures were maintained in Minimum Essential Medium Eagle (MEM, M2279, Sigma) containing 10% Nu serum (BD Biosciences), 30 nM Gentamicin (G1397, Sigma), 2 mM L-glutamine, 4.3 mM insulin and 15 mM glucose (MEM 10%). The preparation was stained with the calcium indicator OGB-1 (Invitrogen—Molecular Probes). To each 50 μg vial of the indicator, 8 μl of DMSO (Sigma-Aldrich), 2 μl 20% Pluronic in DMSO (F-127, Biotium Inc.), and 90 μl of cell medium were added. Dye solution was then added to the cell culture to a final concentration of 2.64 μM (20 μl/3 ml) for an incubation period of 35–40 min after which dye wash out was performed. The culture was then moved to a recording chamber and perfused with oxygenated (95% O_2 and 5% CO_2) artificial cerebrospinal fluid (aCSF) containing (in mM): NaCl, 123; KCl, 3; $NaHCO_3$, 26; NaH_2PO_4, 1; $CaCl_2$, 2; $MgSO_4$ 1.5 and D-glucose [27]. Calcium imaging was performed through the inverted microscope (TE2000U, Nikon) using a CCD camera (C8484–05G, Hamamatsu Photonics), at a frame rate of 10 frames s^{-1}. In each stimulation run, six light pulses with gradually increasing power were projected at inter-pulse intervals of 20 or 30 s (run duration: 2 or 3 min, respectively).

2.2.2. Slice cultures. Slice cultures were prepared from 10–12 day postnatal Sprague Dawley rats' brains, following a protocol similar to Tyler *et al* [28]. Prior to each experiment, a number of slices were loaded with the calcium-sensitive indicator Fluo-4 AM (Molecular Probes, Invitrogen, and Fanbo Biochemicals)—to each 50 μg vial of the dye, 8 μl of DMSO, 2 μl 20% Pluronic F-127 in dimethyl sufloxide (DMSO, Biotium) and 90 μl of the cell medium were added. A couple of hours prior to staining, micro-scale particles were dispersed onto the slices (sprinkled gently), and immediately before the staining process, 800 μl of cell medium were added to the top of the insert and 4 μl of the dye solution were deposited near each slice (to a final dye concentration of 4 μM). After 50 min incubation with the dye, both sides of the inserts were washed with cell medium three times. The slice cultures were then returned to the incubator and allowed to rest for 30 min. After the rest period, slices were moved to the recording chamber, which was perfused with oxygenated (95% O_2 and 5% CO_2) aCSF. Calcium imaging induced by photo-thermal stimulation in the stained cell and slice culture was performed at 10 Hz using a CCD camera (GC1380 H, Prosilica). Laser 'on' durations ranging from 20 μs to 1 ms, during which femtosecond pulses heated the particles, were achieved by controlling both the movement of the galvanometrtic mirrors and the transmittance of the Pockels cell.

2.3. Fluorescent microthermal imaging (FMI)

FMI relies on quantum efficiency changes of fluorescent dyes as a function of temperature [29] (typically decreasing as

temperatures rise). In the linear regime, the change in the fluorescence signal follows:

$$\frac{\Delta F}{F_0} = k \cdot \Delta T$$

where F_0 is the fluorescence baseline level, ΔF the signal change and k the linear quenching coefficient. The FMI fluorescent dye tris(2,2'-bipyridine)ruthenium(II) [30, 31] (Sigma-Aldrich, #652407) was used, due to its high quenching coefficient $k = 2.6\%/^{\circ}$K and wide linear temperature range (0–60 °C), which we validated (figure 2(c)). A 0.8 mM concentration of the dye dissolved in a 1:1 mixture of DMSO and water gave a strong fluorescence signal.

To measure temperature changes during the photo-thermal transients, photo-absorbers were dispersed in a thin layer of this mixture (figure 2(a)). To achieve sub-millisecond temporal precision using our slow CCD camera, we applied repetitive excitation laser pulses (800 or 532 nm) and a stroboscopic imaging method (figure 2(b)): the temperature profile was created by acquiring an image frame at different time points, with predetermined latencies relative to the onset of the laser pulse, using short CCD exposure times (250 μs). To compensate for photo-bleaching, a baseline image is acquired once every few cycles (without laser heating), and the relative fluorescence change ($\Delta I/I$) is estimated by comparing the image to a linear interpolation of the two nearest baseline images. The process was repeated twice and averaged (to increase SNR).

2.4. Computational modelling

A computational model which captures both the physical and biophysical properties of the experimental setting was developed to describe laser-induced temperature transients and their effect on nerve cells. In this model we tested a temperature-rate hypothesis wherein a temperature change leads to an effective transmembrane current proportional to the derivative of the temperature w.r.t. time.

To calculate the tissue temperature rise generated by PAINTS experimental conditions, we used an analytical solution to the heat equation around a discrete absorber [32]:

$$\begin{cases} T(r,t) = \frac{P}{4\pi kr} erfc\left(\frac{r}{\sqrt{4\alpha t}}\right) & t < \tau \\ T(r,t) = \frac{P}{4\pi kr}\left[erfc\left(\frac{r}{\sqrt{4\alpha t}}\right) - erfc\left(\frac{r}{\sqrt{4\alpha (t-\tau)}}\right)\right] & t \geqslant \tau \end{cases} \quad (1)$$

where P (W) is the pulse's power, τ (s) is the pulse duration, $\alpha = 1.4 \times 10^{-7}$ (m^2 s^{-1}) is the thermal diffusivity, $k = 0.6$ (W (mK)$^{-1}$) is the thermal conductivity and r(m) is the distance from the centre of the absorber. These theoretical temperature transients were compared to temperature measurements obtained using FMI.

The biophysical properties of a cortical cell (including the fundamental morphological and electrical properties) were simulated using a NEURON model of a layer-5 pyramidal neuron [33], using temperature-dependent induced currents obtained from the temperature-rate model.

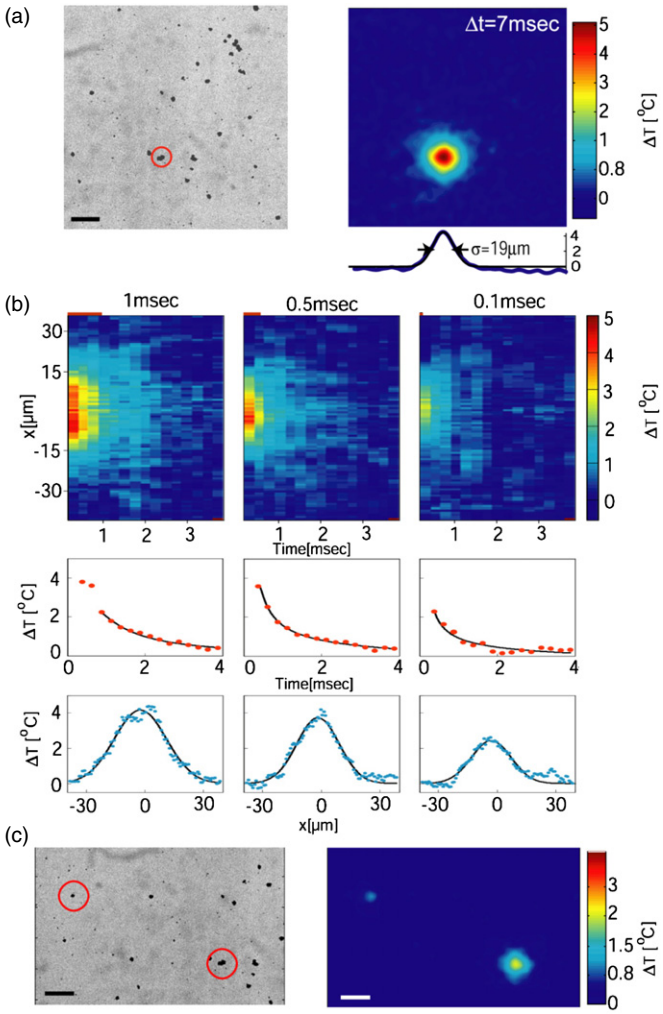

Figure 3. FMI measurements of *PAINTS* temperature transients. (a) Laser-targeted particle in HS I (red circle, left) and smoothed fluorescence $\Delta I/I$ image 7 ms after onset of a 2.5 mW,12 ms illumination pulse (right). Below: horizontal section and Gaussian fit (blue and black lines). (b) Top: Spatio-temporal profiles of thermal transient in HS II following exposure to a 3 mW laser illumination of a microparticle with different durations. Middle: Temporal temperature profiles next to the particle. Bottom: spatial profiles of temperature decay following illumination. (c) Parallel heating of two targeted particles in HS I (red circles, left), Right: $\Delta I/I$ image. Scale bars: 20 μm.

3. Results

3.1. Holographic microscopic thermal transients

To visualize the characteristics of thermal transients experienced by cells around a typical photo-absorber, we imaged temperature profiles using high spatio-temporal resolution stroboscopic FMI [29] of a ruthenium-based dye. These measurements (together with thermal modelling, see section 3.3) demonstrate that almost all the thermal effect of focused illumination pulses is confined to a cellular-scale area of about 12–20 μm radius (figures 3(a)–(c)) and has relaxation times of 0.3–0.6 ms (figure 3(b) middle). The short thermal relaxation times at these scales imply that pulses much shorter than a millisecond are most effective in driving a temperature response without major heat diffusion losses:

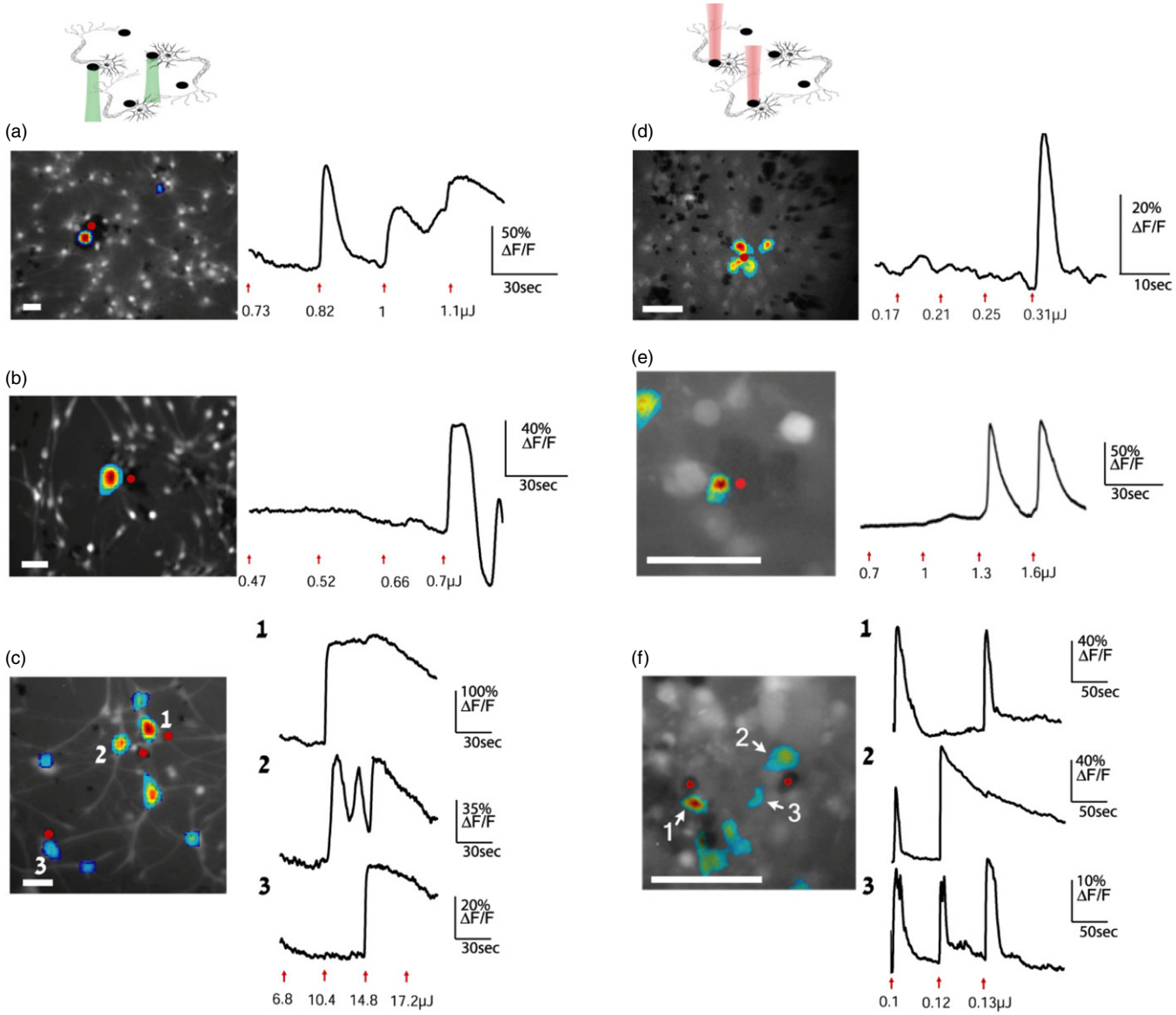

Figure 4. *PAINTS* physiological results in HS I (left panels) and HS II (right panels) for photo-absorbers targeted in the vicinity of cortical cells. The targeted photo-absorbers are marked with red spots and the overlaid colour maps represent the spatial distribution of the peak calcium responses; the line traces show the temporal calcium profile in cells adjacent to targeted photo-absorbers following laser pulses with increasing power (for threshold investigation, red arrows indicate the onset of each stimulus). Calcium responses shown were in cortical cell cultures (panels (a)–(d)) or slice cultures (panels (e) and (f)). Pulse durations were 0.3, 0.08, 3, 0.05, 0.5 and 0.08 ms, respectively. (c) and (f) Calcium transients following multi-focal targeting of a number of particles. Scale bar: 50 μm.

for example, the maximum temperature rise estimated for a 300 nJ, 0.1 ms pulse was only ∼1.7 times smaller than for a 3 μJ pulse lasting 1 ms. Using the SLM to illuminate a multi-focal pattern targeting multiple absorbers induces multiple localized thermal transients with the same spatial–temporal characteristics (figure 3(c)).

3.2. PAINTS physiological results

To examine the ability of the photo-absorber-induced thermal transients to drive neural activity, short pulses (0.02 ms to 1 ms) of intense and highly localized light patterns targeting black micro-particles dispersed in cortical slices and cell cultures were generated (due to their 3D structure, slice culture experiments were only possible on the upright system). Stimulus locked calcium responses in cells adjacent to the targeted particles (figure 4) were observed both in cell culture trials ($n = 47/84$ stimulation experiments on HS I and $n = 127/189$ on HS II) and slice cultures ($n = 83/168$ on HS II). These calcium transients were induced for pulses as short as 0.02 ms when the pulse energies exceeded a certain threshold, with no apparent cellular damage, and are spatially confined to a small region around the targeted particle (figures 4(a)–(d)). Furthermore, using a multi-focal holographic pattern, multiple cells can be activated simultaneously in multiple spatially-confined regions (figures 4(c) and (f); the targeted particles are marked with a red spot). Threshold stimulation levels required for neuronal activation were measured for the different pulse durations (figures 5(a)–(b). The results display a decreasing energy threshold as a function of pulse duration reaching

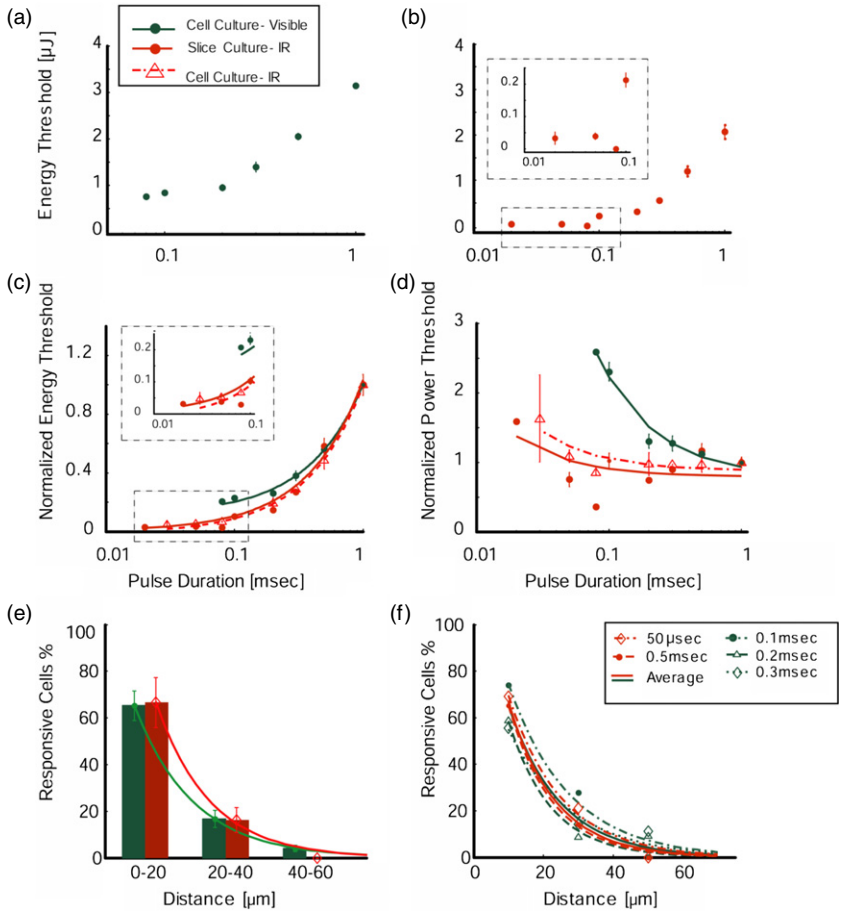

Figure 5. Biophysical characteristics of PAINTS induced responses. (a) and (b) Activation thresholds (total pulse energies) for cell cultures in HS I (a) and slice cultures in HS II(b), as a function of pulse duration. (c) *Normalized* energy thresholds for the different preparations as a function of pulse duration. Inset: magnified view for shorter pulses. (d) Normalized power thresholds for the different preparations. Lines indicate a fit to the Lapicque formula. (e)–(f) The percentage of responsive cell culture cells in the two systems at different radial distance ranges (particle centroid to cell centroid, 0–20 μm, 20–40 μm and 40–60 μm) versus exponential decay fits (solid lines). Response probabilities (within 500 ms from the pulse onset) were measured for several pulse durations in each system and were either (e) pooled together or (f) shown separately ($n = 25$–131 cells for each duration). Threshold and percentage values are reported as mean $\pm$ SE.

a plateau at durations around 200 and $\sim$50 μs for the CW and femtosecond systems, respectively, and with an order of magnitude difference in the plateau threshold energy levels (lower values, down to $<$50 nJ for the femtosecond system). To test whether excitation thresholds are independent of specific environmental factors, we replaced the aCSF perfusion of the cell cultures with MEM 10% media; robust excitation was observed ($n = 74/174$) with nearly identical thresholds (Suppl. figure 1 (available from stacks.iop.org/JNE/10/056004/mmedia)).

To directly compare the behaviour of the different preparations and setups, the energy and the power thresholds were normalized by the mean threshold for 1 ms pulses in each experimental setting, and the data were plotted on the same graph and fitted to a Lapicque strength-duration curve [34] (figures 5(c)–(d)) (with chronaxies of $\sim$160 and $\sim$20 μs for the CW and femtosecond setups, respectively). The normalized cell culture thresholds also behave differently at the different setups: the pulse duration at which the threshold energy and power reaches a plateau is not preparation-dependent but is strongly system-dependent. Finally, to study the dependence of activation probability on a cell's distance from the targeted particle we calculated the percentage of the responsive cells at different increasing radial distances from the particle (figures 5(e)–(f); distances reflect particle centroid to cell centroid; cells responding within 500 ms are included). The results demonstrate an exponential decay of the stimulation probability as the distance increases, emphasizing the high spatial confinement.

3.3. Temperature-rate model for PAINTS responses

Temperature transient measurements (performed as described earlier) were compared to the theoretically predicted transients to validate the discrete absorber assumption. It can be observed from figures 6(a)–(d) that this assumption holds for a varying range of pulse durations (in these figures the circles represent empirical measurements and the solid line represents the solution for the corresponding pulse). It is worth noting that the solution of the heat transfer equation (equation (1)) strengthens the claim that induced thermal transients are confined both spatially (figure 6(a)) and temporally (figure 6(b)) and that modification of the pulse width reduces the duration of the overall temperature transient, without changing the relaxation

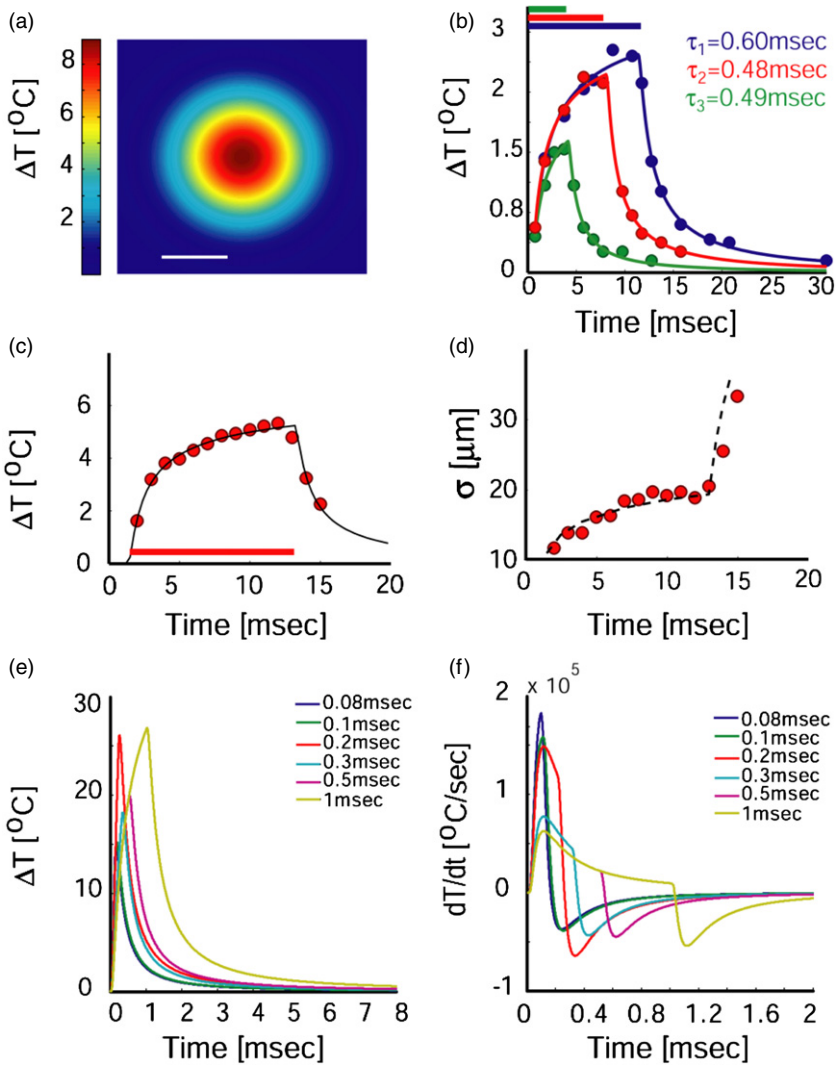

Figure 6. Empirical and theoretical temperature transients in PAINTS experiments. (a) Temperature spatial distribution following a 0.08 ms pulse; scale bar: 10 μm. (b) Temperature measurements (circles) for various pulse durations compared to the theoretical solutions (straight line). Bars indicate pulse durations of 4, 8 and 12 ms. τ_i are measured time constants. (c)–(d) Fluorescence microthermometry of the thermal transient using the visible holographic system for a pulse duration of 14 ms and 2.5 mW. (c) Peak $\Delta I/I$ as a function of time (red circles), fitted with an expression of the form equation (1) (black line). The red bar indicates pulse duration. (d) Width of temperature distribution as a function of time, measured as defined above. The dashed line is a theoretical prediction based on the analytical model, with the blurring effect calculated numerically. (e) Temperature transients calculated under the assumption of a discrete absorber, for various pulse durations and threshold powers measured in the HS I PAINTS experiments (10 μm from the particle's centre). (f) Time derivative of the temperature transients in (e).

time. In addition, to calculate the temperature transients induced under PAINTS experiments, the power thresholds measured in cell culture experiments in the green CW setup for the various pulse durations were substituted into equation (1) and the solution taken at a distance of 10 μm from the centre of the particle (figure 6(e)). The time derivative of these transients is also calculated (figure 6(f)) to be used later for the validation of the temperature-rate model.

Simulation thresholds for the various pulse durations were estimated by inserting scaled temperature derivatives as somatic stimulation currents in the NEURON model. Action potentials were successfully elicited when the scaling factor crossed a certain threshold. Figure 7(a) illustrates the resulting action potentials for increasing scale factors applied to a 0.5 ms pulse—factors lower than the stimulation threshold fail to elicit an action potential. The predicted energy thresholds were calculated by multiplying the simulation power by the threshold scale factor and by the pulse duration, and were compared to the empirical data. Figure 7(b) demonstrates the good fit between empirical data obtained in the green CW setup and predicted energies under the temperature-rate model. When the same model fitting process is applied to the empirical data obtained in the infrared femtosecond setup (for example the slice culture data) it can be observed that for the shorter pulses (shorter than 0.3 ms) the model does not hold (figure 7(c)). The model predictions were also compared to the normalized power measurements for all three preparations (figure 7(d)); a good fit between the model and the data can be observed once again for the longer pulses, which does not hold for the short pulses on the femtosecond setup. This apparent

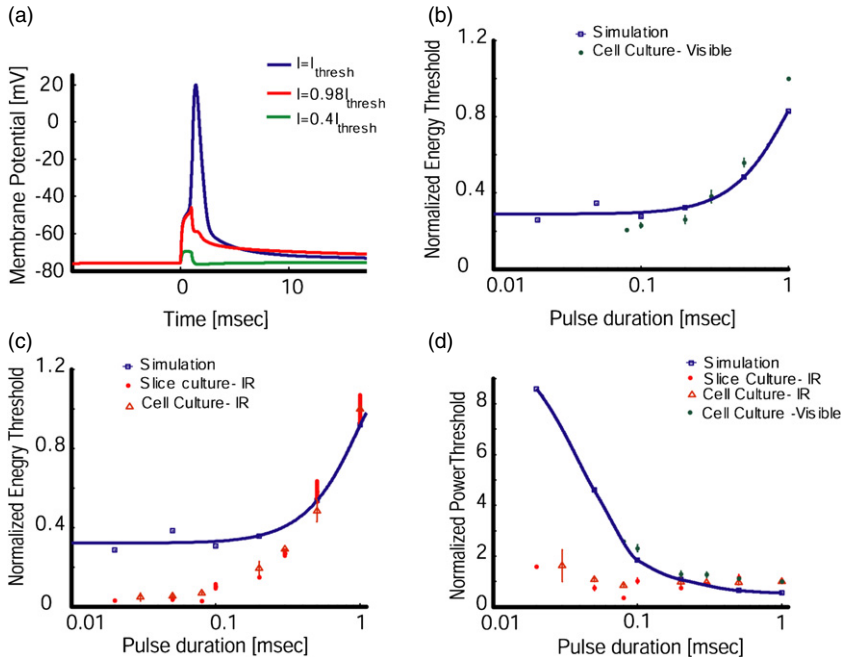

Figure 7. Temperature-rate NEURON model simulation results. (a) membrane potential for a 0.5 ms laser pulse where the induced current was multiplied by different scale factors. (b) and (c) Normalized energy thresholds predicted by the model for varying pulse durations (blue line) compared to the measured energy thresholds for HS I (green) and HS II (red). (d) Normalized *power* thresholds predicted by the model for varying pulse durations (blue) compared to the measured thresholds for the different preparations (red and green). Threshold values are reported as mean ± SE.

discrepancy may be a result of the pulsed nature property of the infrared laser which may lead to the occurrence of an additional laser tissue interaction.

4. Discussion

In this study we explored the feasibility and characteristics of rapid, cellular-precise microscopic photo-thermal neuronal excitation using localized and transient photo-absorption, which may circumvent some of the constraints associated with other currently available optical stimulation methods. Our proof-of-concept measurements (figures 4 and 5) indicate that the biophysical properties of PAINTS appear well-suited for millisecond-timescale cellular-level stimulation with a light budget (10 s of nJ for short excitation pulses) that is comparable to single-photon optogenetic stimulation (typically a few nJ per excitation). Moreover, PAINTS is not constrained to a specific wavelength and can thus be naturally combined with advanced light projection systems (like the holographic systems used here) for high spatiotemporal resolution neuronal stimulation. Moreover, it can employ light at near-IR wavelengths that are weakly absorbed and scattered in biological tissue—in contrast, near-IR multi-photon optogenetic excitation of a single cell is technically challenging, and generally requires power levels of tens of milliwatts for multiple milliseconds per cell [35, 36], that is, ∼100 μJ/spike, or over three orders of magnitude higher than measured PAINTS excitation thresholds. It is interesting to note that our basic observations of photo-absorber mediated excitation are consistent with and extend those of the very recent study by Migliori *et al* [37] using patch recordings in Xenopus oocytes and invertebrate (leech) neurons, using very long pulse durations (50 ms), thus also requiring very high pulse energies (250–3500 μJ).

Using the physiological measurements and a NEURON computer model, we also tested a temperature-rate based hypothesis for the quantitative description of the effects of photo-thermal stimulation on neural tissue. In this model, the thermal changes induce a trans-membrane somatic depolarizing current proportional to the rate of temperature change ($I \propto \mathrm{d}T/\mathrm{d}t$). By employing two experimental setups with very different laser sources in our study, we found that while the *simulation* threshold curves were in very good agreement with the *empirical* photo-thermal activation thresholds obtained in the CW laser stimulation experiments, as well as with the long duration behaviour in the IR femtosecond laser, they fail to predict the results obtained using the IR femtosecond laser for short stimulation pulses. This difference could arise, for example, from non-thermal effects which are not considered by the model; a plausible explanation involves photomechanical effects which may result from pressure pulses generated during the femtosecond pulse absorption or as a result of cavitation around the photo-absorbing particles [38]. Different laser-tissue interaction mechanisms when comparing long (ms) to short (μs) pulses were also noted by Schuele *et al* [39]. Understanding the mechanism underlying thermal activation has major scientific significance in aiding the design of photo-thermal-based neural prosthetics. As a step in this direction, the temperature-rate model was shown here to provide a predictive fit for PAINTS empirical thresholds, but the actual underlying mechanism remains to be clarified. Recently, a highly generic mechanism based on thermally-induced capacitance increases explained

by the Gouy–Chapman–Grahame theory and the capacitive charges phenomenon [40, 41] was introduced as a possible mechanism for photo-thermal stimulation relying solely on the passive properties of the cell membrane and allowing the reliable prediction of thermally induced depolarizations [13]. Thermally induced changes in the membrane capacitance provide a possible explanation for the temperature-rate model resulting from the $V_m \frac{dC_m}{dt}$ component in the membrane current equation. Our results suggest that this relation also holds for millisecond-timescale microscopic thermal transients generated here around microscopic photo-absorbers.

The wavelength flexibility PAINTS provides could allow the use of light that is weakly absorbed and scattered, opening the way towards distributed three-dimension activation in cortical networks. In principle, this flexibility also allows the use of advanced strategies using multiple-colour photo-absorbers, distributed intrinsic photo-absorbers (like blood vessels and/or pigmented tissue) and/or photo-absorbers that are targeted to specific cell types [18, 19, 42]. Holographically patterned photo-stimulation using PAINTS could provide a means for minimally intrusive spatial–temporal control over neuronal dynamics with a high level of spatial and temporal selectivity paving the way towards the development of photo-thermal neural interfaces.

Acknowledgments

The authors gratefully acknowledge the financial support of the European Research Council (grant #211055) and the Israel Science Foundation (1248/06). NF and AZ were supported by fellowships from the Israeli Ministry of Science and Technology, and the David Friedman Fund. We would like to thank Adi Schejter for experimental assistance. We would also like to thank Professor Eitan Kimmel for his helpful discussion.

References

[1] Yizhar O, Fenno L E, Davidson T J, Mogri M and Deisseroth K 2011 Optogenetics in neural systems *Neuron* **71** 9–34

[2] Wells J, Kao C, Mariappan K, Albea J, Jansen E D, Konrad P and Mahadevan-Jansen A 2005 Optical stimulation of neural tissue *in vivo Opt. Lett.* **30** 504–6

[3] Richter C P, Matic A I, Wells J D, Jansen E D and Walsh J T 2010 Neural stimulation with optical radiation *Laser Photon. Rev.* **5** 68–80

[4] Wells J, Kao C, Jansen E D, Konrad P and Mahadevan-Jansen A 2005 Application of infrared light for *in vivo* neural stimulation *J. Biomed. Opt.* **10** 064003

[5] Wells J, Konrad P, Kao C, Jansen E D and Mahadevan-Jansen A 2007 Pulsed laser versus electrical energy for peripheral nerve stimulation *J. Neurosci. Methods* **163** 326–37

[6] Teudt I U, Nevel A E, Izzo A D, Walsh J T Jr and Richter C P 2007 Optical stimulation of the facial nerve: a new monitoring technique? *Laryngoscope* **117** 1641–7

[7] Izzo A D, Richter C P, Jansen E D and Walsh J T Jr 2006 Laser stimulation of the auditory nerve *Lasers Surg. Med.* **38** 745–53

[8] Harris D M, Bierer M, Wells J and Phillips J 2009 Optical nerve stimulation for a vestibular prosthesis *Proc. SPIE* **7180** 71800R

[9] Rajguru S M, Richter C P, Matic A I, Holstein G R, Highstein S M, Dittami G M and Rabbitt R D 2011 Infrared photostimulation of the crista ampullaris *J. Physiol.* **589** 1283–94

[10] Cayce J M, Friedman R M, Jansen E D, Mahavaden-Jansen A and Roe A W 2011 Pulsed infrared light alters neural activity in rat somatosensory cortex *in vivo NeuroImage* **57** 155–66

[11] Wells J, Kao C, Konrad P, Milner T, Kim J, Mahadevan-Jansen A and Jansen E D 2007 Biophysical mechanisms of transient optical stimulation of peripheral nerve *Biophys. J.* **93** 2567–80

[12] Katz E J, Ilev I K, Krauthamer V, Kim do H and Weinreich D 2010 Excitation of primary afferent neurons by near-infrared light *in vitro Neuroreport* **21** 662–6

[13] Shapiro M G, Homma K, Villarreal S, Richter C-P and Bezanilla F 2012 Infrared light excites cells by changing their electrical capacitance *Nature Commun.* **3** 736

[14] Farah N, Brosh I, Butson C R and Shoham S 2012 Photo-thermal neural excitation by extrinsic and intrinsic absorbers: a temperature-rate model, arXiv:1201.4617

[15] Brelen M E, Duret F, Gerard B, Delbeke J and Veraart C 2005 Creating a meaningful visual perception in blind volunteers by optic nerve stimulation *J. Neural Eng.* **2** S22–8

[16] Pezaris J S and Reid R C 2007 Demonstration of artificial visual percepts generated through thalamic microstimulation *Proc. Natl Acad. Sci. USA* **104** 7670–5

[17] Normann R A, Greger B, House P, Romero S F, Pelayo F and Fernandez E 2009 Toward the development of a cortically based visual neuroprosthesis *J. Neural Eng.* **6** 035001

[18] Huang H, Delikanli S, Zeng H, Ferkey D M and Pralle A 2010 Remote control of ion channels and neurons through magnetic-field heating of nanoparticles *Nature Nanotechnol.* **5** 602–6

[19] Barandeh F, Nguyen P-L, Kumar R, Iacobucci G J, Kuznicki M L, Kosterman A, Bergey E J, Prasad P N and Gunawardena S 2012 Organically modified silica nanoparticles are biocompatible and can be targeted to neurons *in vivo PLoS one* **7** e29424

[20] Golan L, Reutsky I, Farah N and Shoham S 2009 Design and characteristics of holographic neural photo-stimulation systems *J. Neural Eng.* **6** 066004

[21] Vaziri A and Emiliani V 2011 Reshaping the optical dimension in optogenetics *Curr. Opin. Neurobiol.* **22** 128–37

[22] Reutsky-Gefen I, Golan L, Farah N, Schejter A, Tsur L, Brosh I and Shoham S 2013 Holographic optogenetic stimulation of patterned neuronal activity for vision restoration *Nature Commun.* **4** 1509

[23] Farah N, Matar S, Marom A, Golan L and Shoham S 2010 *ARVO 2010: Association for Research in Vision and Ophthalmology 2010 Annual Meeting (Fort Lauderdale, FL, 2–6 May)* abstract no. 3470

[24] Farah N 2012 Photo-thermal stimulation for visual restoration: *in vitro* characterization *PhD Thesis* Biomedical Engineering, Technion, Haifa, Israel

[25] Barnes F S 1984 Cell membrane temperature rate sensitivity predicted from the Nernst equation *Bioelectromagnetics* **5** 113–5

[26] Di Leonardo R, Ianni F and Ruocco G 2007 Computer generation of optimal holograms for optical trap arrays *Opt. Express* **15** 1913–22

[27] Ikegaya Y, Le Bon-Jego M and Yuste R 2005 Large-scale imaging of cortical network activity with calcium indicators *Neurosci. Res.* **52** 132–8

[28] Tyler W J, Tufail Y, Finsterwald M, Tauchmann M L, Olson E J and Majestic C 2008 Remote excitation of

neuronal circuits using low-intensity, low-frequency ultrasound *PLoS one* **3** e3511

[29] Barton D L and Tangyunyong P 1996 Fluorescent microthermal imaging: theory and methodology for achieving high thermal resolution images *Microelectronic Eng.* **31** 271–9

[30] Van Houten J and Watts R J 1976 Temperature dependence of the photophysical and photochemical properties of the Tris(2,2'-bipyridyl)ruthenium(II) ion in aqueous solution *J. Am. Chem. Soc.* **98** 4853–8

[31] Van Keuren E, Littlejohn D and Schrof W 2004 Three-dimensional thermal imaging using two-photon microscopy *J. Phys. D: Appl. Phys.* **37** 2938–43

[32] Roider J and Birngruber R 1995 *Optical-Thermal Response of Laser-Irradiated Tissue* ed A J Welch and M J C Martin (New York: Plenum)

[33] Fleidervish I A, Lasser-Ross N, Gutnick M J and Ross W N 2010 Na +imaging reveals little difference in action potential-evoked Na+ influx between axon and soma *Nature Neurosci.* **13** 852–60

[34] Lapicque L 1907 Recherches quantitatives sur l'excitation électrique des nerfs traitée comme une polarization *Physiol. Pathol. Gen.* **9** 620–35

[35] Papagiakoumou E, Anselmi F, Begue A, de Sars V, Gluckstad J, Isacoff E Y and Emiliani V 2010 Scanless two-photon excitation of channelrhodopsin-2 *Nature Methods* **7** 848–54

[36] Packer A M, Peterka D S, Hirtz J J, Prakash R, Deisseroth K and Yuste R 2012 Two-photon optogenetics of dendritic spines and neural circuits *Nature Methods* **9** 1202–5

[37] Migliori B, Di Ventra M and Kristan W Jr 2012 Photoactivation of neurons by laser-generated local heating *AIP Adv.* **2** 032154

[38] Shashkov E V, Everts M, Galanzha E I and Zharov V P 2008 Quantum dots as multimodal photoacoustic and photothermal contrast agents *Nano Lett.* **8** 3953–8

[39] Schuele G, Rumohr M, Huettmann G and Brinkmann R 2005 RPE damage thresholds and mechanisms for laser exposure in the microsecond-to-millisecond time regimen *Invest. Ophthalmol. Vis. Sci.* **46** 714–9

[40] Genet S, Costalat R and Burger J 2000 A few comments on electrostatic interactions in cell physiology *Acta Biotheor.* **48** 273–87

[41] Grahame D C 1947 The electrical double layer and the theory of electrocapillarity *Chem. Rev.* **41** 441–501

[42] Walters R, Kraig R P, Medintz I L, Delehanty J B, Stewart M H, Susumu K, Huston A L, Dawson P E and Dawson G 2012 Nanoparticle targeting to neurons in a rat hippocampal slice culture model *ASN Neuro* **4** e00099